Inorg. Chem. **2006**, *45*, 5455–5464

Inorganic Chemistry
Article

Synthesis, Structure, and Characterization of Molybdenum(VI) Imido Complexes with *N*-Salicylidene-2-aminophenol

Martin Minelli,* Frances Namuswe, Daniel Jeffrey, Amy L. Morrow, Ilia A. Guzei,† Dale Swenson,‡ Eberhard Bothe,§ and Thomas WeyhermÜller§

Department of Chemistry, Grinnell College, Grinnell, Iowa 50112

Received March 6, 2006

Diimido complexes of the type $Mo(NAr)_2Cl_2(dme)$ (dme = 1,2-dimethoxyethane) react with *N*-salicylidene-2-aminophenol ($sapH_2$) in methanol in the presence of 2 equiv of triethylamine to form complexes with the general formula $Mo(NAr)(1,2\text{-}OC_6H_4NH)(sap)$. The structures of three of these compounds (NAr = 2,6-dimethylphenylimido (**1**), 2,4,6-trimethylphenylimido (**2**), 2-*tert*-butylphenylimido(**3**)) have been determined by X-ray crystallography. The coordination sphere around the Mo is a distorted octahedron. The oxygen from the 2-aminophenol is trans to the imido nitrogen, whereas the amido nitrogen and the tridentate sap occupy the four equatorial positions. The Mo–N–C imido linkages have angles of 167.5(2)° (**1**), 163.2(2)° (**2**), and 162.4(1)° (**3**). A precursor complex to the imido–amido complex, $Mo(NAr)(sap)(OCH_3)_2$ (**4**, NAr = 2,4,6-trimethylphenylimido), has been isolated and characterized. Compound **4** reacts with 2-aminophenol to form **2**, with 2-aminothiophenol to form $Mo(NAr)(1,2\text{-}SC_6H_4NH)(sap)$ (**5**), with catechol to form $Mo(NAr)(1,2\text{-}OC_6H_4O)(sap)$ (**6**), with naphthalene-2,3-diol to form Mo(NAr)(naphthalene-2,3-diolate)(sap) (**7**), with 1,2-benzenedithiol to form $Mo(NAr)(1,2\text{-}SC_6H_4S)(sap)$ (**8**), and with 1,2-phenylenediamine to form $Mo(NAr)(1,2\text{-}HNC_6H_4NH)(sap)$ (**9**). The structures of compounds **5**–**9** have been determined by X-ray crystallography. With the exception of compound **8**, the structures are similar to those of **1**, **2**, and **3**, with the bidentate ligand occupying one axial and one equatorial position. In **8**, 1,2-benzendithiolate occupies two equatorial positions, and the nitrogen from sap is located trans to the imido nitrogen. All complexes were characterized by ^1H NMR spectroscopy, cyclic voltammetry, and UV–vis spectroscopy. When a solution of **4** is exposed to moisture-containing air, $MoO_2(sap)(CH_3OH)$ (**10**) is formed. The structure of **10** was also determined.

Introduction

Molybdenum imido complexes have been studied widely over the past years.[1] They are of special interest due to their involvement in the catalysis of olefin metathesis[2] and the Ziegler−Natta olefin polymerization.[3] High-yield synthetic routes for diimido starting materials of the type $Mo(NAr)_2Cl_2(dme)$ (dme = dimethoxyethane)[4] have made it possible to synthesize diimido complexes with a variety of ligands.[5−12] Slight modifications on one of the ligands in an imido complex can have a significant influence on the properties of the compounds. We have shown previously that changing the position of alkyl substituents on the aryl ring

* E-mail: minelli@grinell.edu.

† Current address: Molecular Structure Laboratory, Chemistry Department, University of Wisconsin−Madison, Madison, WI 53558.

‡ Current address: Department of Chemistry, University of Iowa, Iowa City, IA 52242.

§ Current address: Max-Planck Institut für Bioanorganische Chemie, Stiftstrasse 34-36, D-45470 Mülheim, Germany.

(1) (a) Nugent, W. A.; Haymore, B. L. *Coord. Chem. Rev.* **1980**, *31*, 123. (b) Nugent, W. A.; Mayer, J. M. *Metal Ligand Multiple Bonds*; John Wiley & Sons: New York, 1988. (c) Wigley, D. E. *Prog. Inorg. Chem.* **1994**, *42*, 239. (d) Eikey, R. A.; Abu-Omar, M. M. *Coord. Chem. Rev.* **2003**, *243*, 83.

(2) (a) Schrock, R. R.; Hoveyda, A. H. *Angew. Chem., Int. Ed.* **2003**, *42*, 4592. (b) Schrock, R. R. *Chem. Commun.* **2005,** *22*, 2773.

(3) Bolton, P. D.; Mountford, P. *Adv. Synth. Catal.* **2005**, *347*, 355.

(4) Fox, H. H.; Yap, K. B.; Robbins, J.; Cai, S.; Schrock, R. R. *Inorg. Chem.* **1992**, *31*, 2287.

(5) Barrie, P.; Coffey, T. A.; Forster, G. D.; Hogarth, G. *J. Chem. Soc., Dalton Trans.* **1999**, 4519.

(6) Jim A. M.; Brandts, J. A. M.; Boersma, J.; Spek , A. L.; van Koten, G. *Eur. J. Inorg. Chem.* **1999**, *10*, 1727.

(7) Galindo, A.; Montilla, F.; Pastor, A.; Carmona, E.; Gutierrez-Puebla, E.; Monge, A.; Ruiz, C. *Inorg. Chem.* **1997**, *36*, 2379.

(8) Hao, H.; Cui, C.; Bai, G.; Roesky, H. W.; Noltemeyer, M.; Schmidt, H.-G.; Ding, Y. *Z. Anorg. Allg. Chem.* **2000**, *626*, 1660.

(9) Ward, B. D.; Dubberley, S. R.; Gade, L. H.; Mountford, P. *Inorg. Chem.* **2003**, *42*, 4961.

(10) Ramnauth, R.; Al-Juaid, S.; Motevalli, M.; Parkin, B. D.; Sullivan, A. C. *Inorg. Chem.* **2004**, *43*, 4072.

(11) Lokare, K. S.; Ciszewski, J. T.; Odom, A. L. *Organometallics* **2004**, *23*, 5386.

(12) Ciszewski, J. T.; Harrison, J. F.; Odom, A. L. *Inorg. Chem.* **2004**, *43*, 3605.

10.1021/ic060370+ CCC: $33.50 © 2006 American Chemical Society
Published on Web 06/14/2006

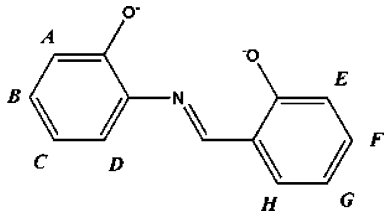

Figure 1. *N*-Salicylidene-2-aminophenolate (sap). Aromatic protons are in italic letters.

of the imido ligand can influence the angle of the imido linkage and the ^{95}Mo NMR chemical shift.[13] In this study, we have used $Mo(NAr)_2Cl_2(dme)$ (NAr = 2,6-dimethylphenylimido, 2,4,6-trimethylphenylimido, 2-*tert*-butylphenylimido) to synthesize imido complexes with the tridentate Schiff base *N*-salicylidene-2-aminophenol ($sapH_2$) (Figure 1). These reactions were expected to lead to either five-coordinate diimido complexes, six-coordinate complexes with a solvent bound in the sixth coordination site, or dimers with bridging and terminal imido ligands, as found for the corresponding oxo-complexes;[14−18] however, the final products were quite different from the compounds we expected.

Experimental Section

All reactions were performed under an argon atmosphere using standard Schlenk techniques unless otherwise noted. The solvents were dried and distilled prior to use. $Mo(NAr)_2Cl_2(dme)$ (H_2NAr = 2,6-dimethylaniline, 2,4,6-trimethylaniline, 2-*tert*-butylaniline) was synthesized according to Schrock et al.,[4] and *N*-salicylidene-2-aminophenol, according to Alyea and Malek.[19] Triethylamine was dried over sodium and distilled prior to use. All other compounds were purchased from Aldrich and were used without further purification. The elemental analyses were carried out by Atlantic Microlab, Inc. in Norcross, GA, and by H. Kolbe, Mülheim (Ruhr), Germany.

Preparation of $Mo(NAr)(1,2\text{-}OC_6H_4NH)(sap)$ (NAr^{2-} = 2,6-Dimethylphenylimido, 1; 2,4,6-Trimethylphenylimido, 2; 2-*tert*-Butylphenylimido, 3). To a suspension of $Mo(NAr)_2Cl_2(dme)$ (1.0 g, 2.0 mmol for **1**, 1.9 mmol for **2**, 1.8 mmol for **3**) in 30 mL of methanol were added 0.43 g (2 mmol) of $sapH_2$ and 0.49 mL (4 mmol) of triethylamine. The mixture was refluxed overnight. The color of the solution changed from dark yellow-brown to dark red-purple. The mixture was cooled to room temperature and filtered. The resulting precipitate was recrystallized in dichloromethane/hexane to yield dark red crystals. The yield, based on $Mo(NAr)_2Cl_2(dme)$, was 0.37 g (35%) for **1**, 0.27 g (26%) for **2**, and 0.23 g (21%) for **3**. ^{1}H NMR for **1** ($(CD_3)_2SO$): δ 14.30 (s, 1), 9.56 (s, 1), 7.92 (d, 1), 7.83 (d, 1), 7.53 (t, 1), 7.18 (t, 1), 7.03 (s, 1), 6.98 (t, 1), 6.92 (d, 1), 6.86 (m, 2), 6.79 (d, 1), 6.67 (t, 1), 6.58 (d, 1), 2.20 (s, 6). Anal. Calcd. for $C_{27}H_{23}MoN_3O_3$, **1**: C, 60.79; H, 4.35; N, 7.87. Found: C, 60.74; H, 4.33; N, 7.88. ^{1}H NMR for **2** ($(CD_3)_2SO$): δ 14.18 (s, 1), 9.51 (s, 1), 7.89 (d, 1), 7.80 (d, 1), 7.50 (t, 1), 7.15 (t, 1), 6.97 (t, 1), 6.89−6.80 (m, 6), 6.77 (d, 1), 6.66 (t, 1), 6.56 (d, 1), 2.25 (s,3), 2.13 (s, 6). Anal. Calcd. for $C_{28}H_{25}MoN_3O_3$, **2**: C, 61.42; H, 4.60; N, 7.67. Found: C, 61.36; H, 4.69; N, 7.59. ^{1}H NMR for **3** ($(CD_3)_2SO$): δ 14.10 (s, 1), 9.56 (s, 1), 7.89 (d, 1), 7.80 (d, 1), 7.53 (t, 1), 7.21 (t, 1), 7.07 (t, 1), 6.96 (m, 8), 6.87 (d, 1), 6.62 (d, 1), 6.05 (d, 1), 1.27 (s, 9). Anal. Calcd. for $C_{29}H_{27}MoN_3O_3\cdot 1/2CH_2Cl_2$, **3**: C, 58.66; H, 4.67; N, 6.95. Found: C, 58.82; H, 4.73; N, 6.87.

Preparation of $Mo(N\text{-}2,4,6\text{-}Me_3C_6H_2)(sap)(OCH_3)_2$ (4). The reaction mixture described above was refluxed for only 2 h instead of overnight. Better yields were obtained if only 0.36 g (1.7 mmol) of $sapH_2$ was used. After 2 h, the reaction mixture was cooled in an ice bath and filtered. The dark brown precipitate, **4**, was dried under vacuum. The yield was 0.30 g (31%). From the red-purple filtrate, black crystals of **2** precipitated out after several hours at room temperature. ^{1}H NMR for **4** ($(CD_3)_2SO$): δ 9.16 (s, 1), 7.78 (d, 1), 7.68 (d, 1), 7.40 (t, 1), 7.13 (t, 1), 6.90 (t, 2), 6.81 (m, 2), 6.67 (s, 2), 3.16 (s, 3), 3.15 (s, 3), 2.15 (s, 3), 2.12 (s, 6). Anal. Calcd. for $C_{24}H_{26}MoN_2O_4$, **4**: C, 57.37; H, 5.22; N, 5.57. Found: C, 56.54; H, 4.88; N, 5.43.

Reactions of 4 with Bidentate Aromatic Ligands. A 0.2-g (0.4 mmol) portion of **4** was reacted with a slight excess (~0.6 mmol) of the aromatic bidentate ligand in 40 mL of methanol. The solution was refluxed for 1 h and then cooled to room temperature. The product was filtered off and dried. For crystals, the product was recrystallized in CH_2Cl_2/hexane. A precipitate does not form with 1,2-phenylenediamine (see below).

2-Aminophenol. Yield: 66% of **2**.

2-Aminothiophenol. Yield: 70% of $Mo(NAr)(1,2\text{-}SC_6H_4NH)(sap)$, **5**. ^{1}H NMR for **5** ($(CD_3)_2SO$): δ 14.43 (s,1), 9.47 (s, 1), 7.83 (d, 1), 7.77 (d, 1), 7.48 (t, 1), 7.15 (m, 2), 7.07 (d, 1), 6.93 (t, 1), 6.87 (m, 5), 6.82 (t, 1), 6.73 (d, 1), 2.27 (s, 3), 2.25 (s, 6). Anal. Calcd. for $C_{28}H_{25}MoN_3O_2S$, **5**: C, 59.67; H, 4.47; N, 4.97. Found: C, 59.25; H, 4.95; N, 6.95.

Catechol. Yield: 90% $Mo(NAr)(1,2\text{-}OC_6H_4O)(sap)$, **6**. ^{1}H NMR for **6** ($(CD_3)_2SO$): δ 9.69 (s, 1), 7.93 (d, 2), 7.64 (t, 1), 7.26 (t, 1), 7.15 (t, 1), 6.86 (m, 3), 6.84 (m, 3), 6.56 (d, 1), 2.28 (s, 3), 2.19 (s, 6). Anal. Calcd. for $C_{28}H_{24}MoN_2O_4$, **6**: C, 61.32; H, 4.41; N, 5.10. Found: C, 60.50; H, 4.36; N, 4.98.

Naphthalene-2,3-diol. Yield: 64% of Mo(NAr)(naphthalene-2,3-diolate)(sap), **7**. ^{1}H NMR for **7** ($(CD_3)_2SO$): δ 9.73 (s, 1), 7.97 (m, 2), 7.69 (m, 3), 7.28 (m, 9), 6.90 (s, 2), 2.31 (s, 3), 2.28 (s, 6). Anal. Calcd. for $C_{32}H_{26}MoN_2O_4$, **7**: C, 64.21; H, 4.38; N, 4.68. Found: C, 63.70; H, 3.82; N, 4.15.

Benzene-1,2-dithiol. Yield: 60% of $Mo(NAr)(1,2\text{-}SC_6H_4S)(sap)$, **8**. ^{1}H NMR for **8** ($(CD_3)_2SO$): δ 9.92 (s, 1), 8.10 (t, 2), 7.76(t, 1), 7.36(t, 1), 7.14 (m, 6), 6.98 (s, 2), 6.94 (m, 2), 2.43 (s, 6), 2.34 (s, 3). Anal. Calcd. for $C_{28}H_{24}MoN_2O_2S_2$, **8**: C, 57.92; H, 4.17; N, 4.82. Found: C, 57.48; H, 4.23; N, 4.28.

1,2-Phenylenediamine. The synthesis was carried out as described above, but no precipitate formed. When the solvent was evaporated, an amorphous solid remained. This solid was recrystallized in THF and CH_2Cl_2. The formation of crystals was aided by adding a small amount of acetone. Yield: ~5% of $Mo(NAr)(1,2\text{-}HNC_6H_4NH)(sap)$, **9**. ^{1}H NMR for **9** ($(CD_3)_2SO$): δ 13.15 (s, 1), 9.69 (s, 1), 9.46 (s, 1), 7.86 (d, 1), 7.84 (d, 1), 7.42 (t, 1), 7.11 (t, 1), 6.8 (m, 6), 6.75 (m, 2), 6.5 (unres, 1), 6.35 (unres, 1), 2.25 (s, 3), 2.14 (s, 6). Anal. Calcd. for $C_{28}H_{26}MoN_4O_2$, **9**: C, 61.54; H, 4.80; N, 10.25. Found: C, 61.42; H, 4.87; N, 10.25.

Synthesis of $MoO_2(sap)(CH_3OH)$. When the filtrate from the synthesis of **4** (above) is exposed to moisture-containing air, in addition to **2**, orange crystals of $MoO_2(sap)(CH_3OH)$, **10**, form and can be isolated. ^{1}H NMR for **10** ($(CD_3)_2SO$): δ 9.26 (s, 1), 7.82

(13) Minelli, M.; Hoang, M. L.; Kraus, M.; Kucera, G.; Loertscher, J.; Reynolds, M.; Timm, N.; Chiang, M. Y.; Powell, D. *Inorg. Chem.* **2002**, *41*, 5954−5960.
(14) Syamal, A.; Maurya, M. R. *Coord. Chem. Rev.* **1989**, *95*, 183.
(15) Mondal, J. U.; Schultz, F. A.; Brennan, T. D.; Scheidt, W. R. *Inorg. Chem.* **1988**, *27*, 3950.
(16) Rajan, O. A.; Chakravorty, A. *Inorg. Chem.* **1981**, *20*, 660.
(17) Craig, J. A.; Harlan, E. W.; Snyder, B. S.; Whitener, M. A.; Holm, R. H. *Inorg. Chem.* **1989**, *28*, 2082.
(18) Cindric, M.; Strukan, M.; Vrdoljak, V.; Kamenar, B. *Z. Anorg. Allg. Chem.* **2004**, *630*, 585.
(19) Alyea, E. C.; Malek, A. *Can. J. Chem.* **1975**, *53*, 939.

(d, 1), 7.79 (d, 1), 7.54 (t, 1), 7.23 (t, 1), 7.08 (t, 1), 7.00 (m, 3), 6.87 (d, 1), 6.62 (d, 1), 6.05 (d, 1), 3.16, 3.14 (2s, 3). Anal. Calcd. for $C_{14}H_{12}MoNO_5$, **10**: C, 45.42; H, 3.27; N, 3.78. Found: C, 45.65; H, 3.48; N, 3.81.

NMR Spectroscopy. The ^{1}H NMR spectra were measured on a Bruker 400-MHz DRX spectrometer and a Bruker 500-MHz DRX spectrometer at room temperature. The residual solvent was used as an internal reference for chemical shift determination.

Infrared Spectroscopy. The IR spectrum of **10** was measured on a Perkin-Elmer System 2000 infrared spectrometer as KBr pellet.

Electrochemistry. (a) The cyclic voltammograms of **1**−**3** were recorded using a PAR 175 Universal Programmer and a PAR 173 Potentiostat. The three-electrode electrochemical cell consisted of a platinum disk working electrode, a platinum wire auxiliary electrode, and a silver electrode as a reference electrode. The potentials are reported as potentials vs silver wire and were corrected to potentials vs ferrocene as an internal standard. The complexes were dissolved (5×10^{-4} M) in acetonitrile in the presence of 0.1 M tetrabutylammonium tetrafluoroborate as electrolyte.

(b) Cyclic voltammograms of the complexes were also recorded at room temperature in solutions of CH_3CN containing 0.2 M [(*n*-Bu)$_4$N]PF_6 (TBAHFP) as supporting electrolyte. Potential control was achieved using an E.G.&G. potentiostat/galvanostat (model 273A) and M270 software. For the measurements, a conventional three-electrode arrangement was employed that consisted of a glassy carbon electrode (2-mm diameter), a Ag/Ag$^+$ (0.01 M $AgNO_3$) reference electrode, and a Pt wire counter electrode. Small amounts of ferrocene were added as an internal standard after completion of each set of experiments, and potentials are referenced versus the ferrocenium/ferrocene (Fc$^+$/Fc) couple.

Spectroelectrochemistry. (a) A HP 8452 diode array spectrometer with a deuterium lamp and a PAR 173 potentiostat were used, together with an OTTLE cell that had three electrodes: an OTTLE as the working electrode, a silver wire as reference electrode, and a platinum wire as a counter electrode. A 3-mL reservoir held the solution and the two latter electrodes. The potentiostat was set at 5 mV/s, and the spectra were taken after every 0.02 V at 2−3-min intervals.[20] Solvent and electrolyte were the same as in part a, above.

(b) Controlled potential electrolysis of 8 mL off solution was performed at −25 °C in a jacketed quartz cuvette with a Ag/Ag$^+$ (0.01 M $AgNO_3$) reference electrode, a Pt mesh working electrode, and a Pt brush counter electrode. The latter was mounted in its own compartment, which was separated from the electrolysis solution by a Vycor frit. The potential for coulometry was chosen ∼0.2 V more negative than the respective reduction potential. Mixing of the solution during the coulometry was achieved by bubbling argon through the solution. The 0.5-cm cuvette was mounted in a Hewlett-Packard HP 8453 spectrophotometer. UV−vis spectra were recorded in situ during the electrolysis. After the completion of the electrolysis, samples of the electrolyzed solutions were taken with gastight syringes and frozen rapidly for EPR analysis.

EPR Spectroscopy. The room-temperature EPR spectra were measured on a Varian E-6 spectrometer using a quartz flat cell. The low-temperature EPR spectra were measured on a 9.43-GHz Bruker E500 spectrometer using 4-mm quartz tubes.

UV−vis Spectroscopy. The UV−vis spectra were measured on a Perkin-Elmer Lamda 19 spectrophotometer using 0.1-cm quartz cells. The concentrations were around 1×10^{-4} M in CH_3CN.

X-ray Crystallographic Data Collection and Refinement of the Structures. Crystallographic data of the compounds are listed in Table 1.

Complex 1. A dark purple blade (0.05 × 0.11 × 0.40 mm) of **1** was isolated from the sample and mounted with grease on the tip of a glass capillary epoxied to a brass pin and placed on the diffractometer with the long crystal dimension (*a* axis) approximately parallel to the diffractometer φ axis. Data for **1** were collected on an Nonius Kappa CCD diffractometer (Mo K_α radiation, graphite monochromator) at 190 K (cold N_2 gas cooling) using standard CCD techniques, yielding 29 627 data points. Lorentz and polarization corrections were applied. An empirical absorption correction was applied using the multiscan technique. Equivalent data were averaged, yielding 5257 unique data points (R-int = 0.045, 4278 > 4 *sigma(F)). On the basis of preliminary examination of the data, the space group *Pbca* was assigned (no significant exceptions to the *hk*0, *h* = odd; *h*0*l*, *l* = odd; 0*kl*, *k* = odd systematic absences were noted). The computer programs from the HKL2000 package were used for data reduction. The preliminary model of the structure was obtained using XS, a direct methods program. Least-squares refining of the model vs the data was done with the XL computer program. Illustrations were made with the XP program, and tables were made with the XCIF program. All are in the SHELXTL, v5.1 package. Thermal ellipsoids are drawn at the 35% level unless otherwise noted.

All non-hydrogen, nondisordered atoms were refined with anisotropic thermal parameters. The tridentate ligand was positionally disordered. The ligand's major site (occ = 0.726(5)) is designated with atom labels O1−O14 and was refined with anisotropic thermal parameters. The ligand's minor site (occ = 0.274(5)) is approximated by a 180° rotation of the major site about an axis defined by the Mo1−(C7−N8 bond midpoint) vector. The atom labels O1′−O14′ are used for the minor site. The conformation of the minor site was constrained to be the same as that of the major site. A group isotropic thermal parameter for all non-hydrogen atoms of the minor site was used in the refinement model. Hydrogen atom H7 was allowed to refine as an independent isotropic atom. All remaining H atoms (including those with partial occupancy) were included in the final refinement using the riding model with default parameters.

Complexes 2 and 3. Red crystals of **2** and **3** were selected under paratone oil under ambient conditions and attached to the tip of a nylon loop. The crystals were mounted in a stream of cold nitrogen at 100(2) K and centered in the X-ray beam by using a video camera.

The crystal evaluation and data collection were performed on a Bruker CCD-1000 diffractometer with Mo K_α (λ = 0.71073 Å) radiation and the diffractometer-to-crystal distance of 4.9 cm. The initial cell constants were obtained from three series of ω scans at different starting angles. Each series consisted of 20 frames collected at intervals of 0.3° in a 6° range about ω with the exposure time of 10 s per frame. The harvested reflections were successfully indexed by an automated indexing routine built in the SMART program. The final cell constants were calculated from a set of 20 610 strong reflections for **2** and 1002 for **3** from the actual data collection. The reciprocal space was surveyed to the extent of a full sphere to a resolution of 0.80 Å. A total of 41 347 data points were harvested by collecting seven sets of frames with 0.3° scans in ω with an exposure time 20 s per frame for **2** and 30 s per frame for **3**. These highly redundant datasets were corrected for Lorentz and polarization effects. The absorption correction was based on fitting a function to the empirical transmission surface as sampled by multiple equivalent measurements.[21] The systematic absences in

(20) DeAngelis, T. P.; Heinemann, W. R. *J. Chem. Educ.* **1976**, *53*, 594.

(21) Bruker-AXS. (2000−2003) SADABS V.2.05, SAINT V.6.22, SHELXTL V.6.10, and SMART 5.622 Software Reference Manuals; Bruker-AXS: Madison, WI.

Table 1. Crystallographic Data for **1**, **2**, **3**·0.5CH_2Cl_2, **5**, **6**, **7**, **8**, **9**·acetone, and **10**

	1	**2**	**3**·0.5 CH_2Cl_2	**5**	**6**
chem formula	$C_{27}H_{23}MoN_3O_3$	$C_{28}H_{25}MoN_3O_3$	$C_{29.5}H_{28}ClMoN_3O_3$	$C_{28}H_{25}MoN_3O_2S$	$C_{28}H_{24}MoN_2O_4$
fw	533.42	547.45	603.94	563.51	548.43
space group	*Pbca*, No. 61	$P2_1/n$, No. 14	*Pbca*, No. 61	$P2_1/n$, No. 14	$P2_1/n$, No. 14
a, Å	8.3385 (3)	8.5450 (11)	12.6310 (14)	8.2851 (2)	13.9504 (5)
b, Å	20.9434(6)	16.939 (2)	17.211 (2)	17.1205 (5)	9.9723 (3)
c, Å	26.3109 (9)	16.750 (2)	24.356 (3)	17.5495 (5)	17.1114 (6)
α, deg	90	90	90	90	90
β, deg	90	101.838 (2)	90	99.822 (5)	90.256 5)
γ, deg	90	90	90	90	90
V, Å	4594.8 (3)	2372.9 (5)	5249.9 (10)	2452.82 (12)	2380.47 (14)
Z	8	4	8	4	4
T, K	190 (2)	100 (2)	100 (2)	100 (2)	100 (2)
ρ calcd, g cm^{-3}	1.542	1.532	1.515	1.526	1.530
reflns collected/$2\Theta_{max}$	69374/55.0	41347/52.92	41703/52.76	71627/68.60	83529/70.00
unique reflns/$I > 2\sigma$(I)	6257/4278	4890/4594	5418/4828	10215/8651	10436/9412
no. of params/restr	367/42	327/0	311/0	368/45	368/45
λ, Å/*μ*(Kα), cm^{-1}	0.71073/6.06	0.71073/5.89	0.71073/6.33	0.71073/6.51	0.71073/5.89
R1[a]/GOF[b]	0.0604/1.257	0.0370/1.132	0.0349/1.028	0.0383/1.057	0.0309/1.120
wR2[c] ($I > 2\sigma$ (I))	0.0887	0.0883	0.0774	0.0836	0.0672
residual density, e$Å^{-3}$	0.42/−0.43	0.76/0.62	1.03/−0.71	+1.47/−2.13	+0.72/−0.55

	7	**8**	**9**·Acetone	**10**
chem formula	$C_{32}H_{26}MoN_2O_4$	$C_{28}H_{24}MoN_2O_2S_2$	$C_{31}H_{32}MoN_4O_3$	$C_{14}H_{13}MoNO_5$
fw	598.49	580.55	604.55	371.19
space group	$P2_1/n$, No. 14	$P\bar{1}$, No. 2	$P2_1/c$, No. 14	$P2_1/n$, No. 14
a, Å	14.2100 (7)	10.2268 (7)	8.8469 (5)	11.4839 (6)
b, Å	9.9737 (4)	10.5520 (8)	12.7485 (7)	6.7543 (4)
c, Å	18.9907 (9)	13.0500 (11)	25.1199 (14)	17.5715 (9)
α, deg	90	74.123(4)	90	90
β, deg	101.339 (5)	67.455 (4)	99.995 (5)	92.878 (5)
γ, deg	90	75.855(5)	90	90
V, Å	2638.9 (2)	1235.5 (2)	2790.1 (3)	1361.23 (13)
Z	4	2	4	4
T, K	100 (2)	100 (2)	100 (2)	100 (2)
ρ calcd, g cm^{-3}	1.506	1.561	1.439	1.811
reflns collected/$2\Theta_{max}$	24122/52.00	16935/55.00	21653/60.00	32182/62.00
unique reflns/$I > 2\sigma$(I)	5176/3909	5659/4297	7440/5638	4339/3581
no. of params/restr	324/42	319/8	358/6	201/0
λ, Å/*μ*(Kα), cm^{-1}	0.71073/5.39	0.71073/7.29	0.71073/5.09	0.71073/9.85
R1[a]/GOF[b]	0.0434/1.057	0.0417/1.033	0.0544/1.065	0.0326/1.069
wR2[c] ($I > 2\sigma$ (I))	0.0729	0.0699	0.1391	0.0692
residual density, e$Å^{-3}$	+0.56/−0.43	+0.42/−0.49	+0.99/−1.32	+1.53/−0.67

[a] Observation criterion: $I > 2\sigma(I)$. $R1 = \sum||F_o| - |F_c||/\sum|F_o|$, [b] $GOF = [\sum[w(F_o^2 - F_c^2)^2]/(n - p)]^{1/2}$ [c] $wR2 = [\sum[w(F_o^2 - F_c^2)^2]/\sum[w(F_o^2)^2]]^{1/2}$, where $w = 1/\sigma^2(F_o^2) + (aP)^2 + bP$, $P = (F_o^2 + 2F_c^2)/3$.

the diffraction data were uniquely consistent for the space group $P2_1/n$ for **2** and *Pbca* for **3**; these space groups yielded chemically reasonable and computationally stable results of refinement.

Successful solutions by the direct methods provided most non-hydrogen atoms from the *E*-map. The remaining non-hydrogen atoms were located in an alternating series of least-squares cycles and difference Fourier maps. All non-hydrogen atoms were refined with anisotropic displacement coefficients. All hydrogen atoms were included in the structure factor calculation at idealized positions and were allowed to ride on the neighboring atoms with relative isotropic displacement coefficients. In the structure of **2**, the tridentate ligand is disordered in a 2:1 ratio over two positions, a fact manifested in somewhat enlarged thermal motion ellipsoids of some of the atoms within the ligand and in well-resolved positional disorder of atoms N3 and C22. The latter were refined with soft restraints. In the structure of **3**, there is also one-half molecule of solvate dichloromethane per Mo complex present in the lattice. The solvate dichloromethane molecule is disordered over a crystallographic inversion center.

Complexes 5−10. Deep red to black single crystals of **5**, **6**, **7**, **8**, **9** and a yellow specimen of **10** were coated with perfluoropolyether and mounted in the nitrogen cold stream of a Nonius Kappa-CCD diffractometer equipped with a Mo-target rotating-anode X-ray source and a graphite monochromator (Mo−Kα, $\lambda = 0.71073$ Å). Final cell constants were obtained from least-squares fits of all measured reflections. Crystal faces of sample **6** were determined, and the corresponding intensity data were corrected for absorption using the Gaussian-type routine embedded in XPREP.[22] The Siemens ShelXTL[22] software package was used for solution and artwork of the structure, and ShelXL97[23] was used for the refinement. The structures were readily solved by direct and Patterson methods and subsequent difference Fourier techniques.

All non-hydrogen atoms were refined anisotropically, except disordered atoms of the sap-ligand in **7**, which were isotropically refined. Hydrogen atoms attached to carbon atoms were placed at calculated positions and refined as riding atoms with isotropic displacement parameters. To determine the degree of protonation, acidic hydrogen atoms attached to nitrogen were located from the difference map and were then refined as riding atoms with corresponding HFIX instructions. The OH proton of the coordinated methanol molecule in compound **10** was easily located from the

(22) ShelXTL, V. 5. Siemens Analytical X-ray Instruments, Inc.: Madison, WI, 1994.
(23) ShelXL97. G. M. Sheldrick; University of Göttingen: Göttingen, Germany, 1997.

Table 2. Selected Bond Lengths (Å) and Bond Angles (°) for **1**, **2**, and **3**

compd	1	2	3
Mo−N(1)	1.750(3)	1.751(2)	1.7488(17)
Mo−O(1)	2.076(2)	2.0744(18)	2.0540(14)
Mo−N(2)	1.975(3)	1.977(2)	1.9823(16)
Mo−N(3)	2.214(3)	2.199(3)	2.2090(17)
Mo−N(3′)	2.218(6)		
Mo−O(2)	1.939(3)	1.978(2)	1.9828(14)
Mo−O(2′)	1.868(7)		
Mo−O(3)	2.039(3)	1.993(2)	2.0089(14)
Mo−O(3′)	2.091(7)		
Mo−N(1)−C(1)	167.5(2)	163.20(18)	162.40(14)
N(1)−Mo−O(2)	166.68(10)	162.71(8)	162.73(7)
O(3)−Mo−O(2)	156.7(3)	155.10(11)	153.30(6)
O(3′)−Mo−O(2′)	156.7(3)		
O(3)−Mo−N(3)	74.96(12)	71.48(12)	75.71(6)
O(3′)−Mo−N(3′)	73.9(2)		
N(1)−Mo−N(3)	103.06(12)	101.99(10)	95.65(7)
N(1)−Mo−N(2)	90.94(11)	88.67(9)	89.90(7)
N(1)−Mo−O(2)	99.63(13)	96.60(9)	94.08(7)
N(1)−Mo−O(3)	98.06(15)	101.00(10)	103.42(7)

difference map. An isotropic displacement parameter of 1.3 times U_{eq} of the O-atom was used.

All structures suffered from disorder of the sap−ligand, which was found to be present in both of the two possible bite orientations. A split atom model was used to account for the disorder. Equal thermal displacement parameters were refined for the split positions (EADP Instruction), and geometrical restraints were introduced for corresponding distances and angles of the SIP−ligand (SAME and SADI instruction).

Results and Discussion

Syntheses and Structures. The reaction of $Mo(NAr)_2Cl_2(dme)$ with $sapH_2$ in methanol in the presence of 2 equiv of triethylamine produces $Mo(NAr)(1,2\text{-}OC_6H_4NH)(sap)$. The yields are around 25%, based on the molybdenum starting material. Crystals of three complexes with different alkyl substituents on the imido ligand (NAr = 2,6-dimethylphenylimido, **1**; 2,4,6-trimethylphenylimido, **2**; 2-*tert*-butylphenylimido, **3**) were obtained, and the structures were determined by X-ray crystallography. The crystallographic data for compounds **1**, **2**, and **3** are listed in Table 1, selected bond lengths and bond angles, in Table 2. Figure 2 shows a molecular drawing of complex **2**. In compounds **1**−**3**, the coordination sphere around the Mo is a distorted octahedron. The imido linkages have angles of 167.5(2)° in **1**, 163.2(2)° in **2**, and 162.4(1)° in **3** and can be considered linear.[5] Each Mo center is also bound to an amido and an imine nitrogen. The bond lengths increase from $Mo-N_{imido}$ (1.75 Å) to $Mo-N_{amido}$ (1.98 Å) and $Mo-N_{imine}$ (2.20 Å), as expected. The oxygen from the 2-aminophenol is trans to the imido nitrogen, whereas the amido nitrogen and the tridentate sap occupy the four equatorial positions. No lengthening of the Mo−O bond trans to the imido linkage is observed. Such a trans influence is seen in $Mo(NAr)Cl_2(dtc)_2$ complexes,[13] for example. Since the sap ligand does not have a C_2 axis, the structures reported here have disorders with regard to inversion of the sap ligand. Mondal et al.[15] also found disorder in crystals of MoO(naphthalene-2,3-diolato)(sap).

The presence of the 2-aminophenol ligand in the complex was surprising. Since five-coordinate diimido complexes

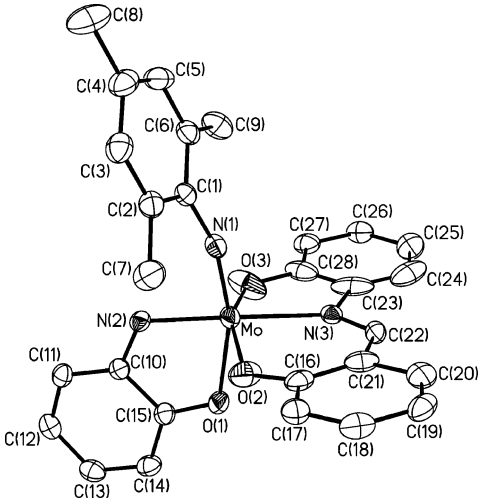

Figure 2. Molecular drawing of $Mo(N(2,4,6\text{-}Me_3)C_6H_2)(1,2\text{-}OC_6H_4NH)(sap)$, **2**.

Scheme 1. Proposed Reaction Mechanism for the Formation of **4**

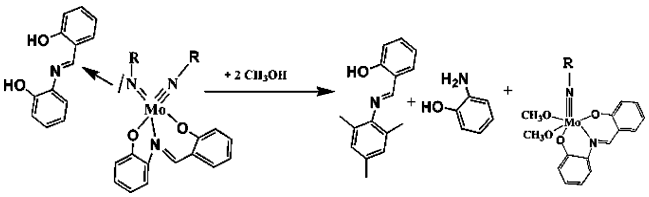

have been obtained under similar conditions,[6,8,12] we expected $Mo(NAr)_2(sap)$ as the product. When the reaction mixture is refluxed for only 2 h, a brown complex can be isolated. Efforts to grow crystals of this complex have been unsuccessful. The complex is fairly stable in coordinating solvents, but it decomposes in others. On the basis of the ^1H NMR spectrum and the elemental analysis, the complex can be formulated as $Mo(N\text{-}2,4,6\text{-}Me_3C_6H_2)(sap)(OCH_3)_2$, **4**. In methanol, **4** can be reacted with 2-aminophenol to form **2** with a 60% yield.

On the basis of the data above, we suggest the following pathway for the reaction of $Mo(NAr)_2Cl_2(dme)$ with $sapH_2$ in the presence of 2 equiv of base. First a diimido complex with sap is formed (eq 1). The imine carbon of another $sapH_2$ then reacts with one of the imido nitrogens to form a new Schiff base, $HOC_6H_4CH{=}N\text{-}2,4,6\text{-}Me_3{-}C_6H_2$, 2-aminophenol, and **4** (eq 2, Scheme 1). Compound **4** then reacts with 2-aminophenol to form the imido−amido complex, **2** (eq 3).

$$Mo(NAr)_2Cl_2(dme) + sapH_2 + 2NEt_3 \rightarrow Mo(NAr)_2(sap) + 2NEt_3HCl + dme \quad (1)$$

$$Mo(NAr)_2(sap) + sapH_2 + 2CH_3OH \rightarrow Mo(NAr)(sap)(OCH_3)_2\ (\mathbf{4}) + HOC_6H_4CH{=}NC_6H_2(2,4,6\text{-}Me_3) + 1,2\text{-}HOC_6H_4NH_2 \quad (2)$$

$$Mo(NAr)(sap)(OCH_3)_2\ (\mathbf{4}) + 1,2\text{-}HOC_6H_4NH_2 \rightarrow Mo(NAr)(1,2\text{-}OC_6H_4NH)(sap)\ (\mathbf{2}) + 2CH_3OH \quad (3)$$

Although the proposed mechanism requires a 2:1 ratio of $sapH_2/Mo(NAr)_2Cl_2(dme)$, the synthesis was carried out in

Table 3. Selected Bond Lengths (Å) and Bond Angles (°) for **5**, **6**, **7**, **8**, **9**

compd	**5**	**6**	**7**	compd	**8**	**9**
Mo(1)−N(31)	1.7628 (15)	1.7585 (10)	1.761 (3) (N(41))	Mo(1)−N(31)	1.734 (2)	1.744 (2)
Mo(1)−O(1)	1.9197 (19)	1.921 (4)	1.902 (5)	Mo(1)−O(1)	1.93 (5)	1.989 (5)
Mo(1)−O(1′)	1.889 (4)	1.907 (3)	1.874 (6)	Mo(1)−O(1′)	1.967 (6)	1.992 (6)
Mo(1)−N(9)	2.2244 (19)	2.211 (2)	2.205 (5)	Mo(1)−N(9)	2.310 (5)	2.244 (5)
Mo(1)−N(9′)	2.227 (3)	2.1961 (18)	2.199 (5)	Mo(1)−N(9′)	2.256 (5)	2.204 (5)
Mo(1)−O(16)	2.060 (2)	2.000 (4)	2.010 (5)	Mo(1)−O(16)	1.967 (6)	2.002 (5)
Mo(1)−O(16′)	2.100 (3)	2.001 (3)	1.997 (6)	Mo(1)−O(16′)	1.985 (5)	2.004 (6)
Mo(1)−N(28)	1.9779 (13)			Mo(1)−S(28)	2.4075 (8)	
Mo(1)−O(28)		1.9514 (9)	1.938 (2) (O(32))	Mo(1)−N(28)		2.077 (2)
Mo(1)−S(21)	2.5001 (5)			Mo(1)−S(21)	2.4333 (8)	
Mo(1)−O(21)		2.0859 (9)	2.080 (2)	Mo(1)−N(21)		1.970 (2)
Mo(1)−N(31)-C(32)	167.58 (12)	174.11 (9)	178.0 (3) (1−41−42)	Mo(1)−N(31)-C(32)	178.1 (2)	167.4 (2)
N(31)−Mo(1)-S(21)	167.12 (5)			N(31)−Mo(1)-S(21)	101.45 (8)	
N(31)−Mo(1)-O(21)		171.04 (4)	174.32 (11)	N(31)−Mo(1)-N(21)		90.79 (11)
O(1)−Mo(1)-O(16)	156.76 (8)	153.45 (14)	152.51 (19)	O(1)−Mo(1)-O(16)	111.7 (6)	153.3 (3)
O(1′)-Mo(1)−O(16)	13.08 (11)	11.67 (11)	13.0 (2)	O(1′)-Mo(1)−O(16)	9.1 (11)	11.3 (4)
O(1)−Mo(1)-N(31)	94.01 (8)	98.39 (14)	99.08 (18) (N(41))	O(1)−Mo(1)-N(31)	101.2 (3)	100.5 (3)
O(1′)-Mo(1)−N(31)	99.33 (15)	96.74 (14)	93.7 (2) (N(41))	O(1′)-Mo(1)−N(31)	93.3 (5)	101.9 (6)
N(28)−Mo(1)-N(31)	89.36 (6)			S(28)−Mo(1)-N(31)	101.42 (8)	
O(28)−Mo(1)-N(31)		93.63 (4)	100.21 (18) (32−1−41)	N(28)−Mo(1)-N(31)		165.85 (11)
N(28)−Mo(1)-N(9)	161.06 (6)			S(28)−Mo(1)-N(9)	97.25 (15)	
O(28)−Mo(1)-N(9)		161.34 (6)	158.67 (13) (32−1−9)	N(28)−Mo(1)-N(9)		95.47 (13)
N(28)−Mo(1)-O(1)	104.56 (7)			S(28)−Mo(1)-O(1)	104.56 (7)	
O(28)−Mo(1)-O(1)		108.99 (8)	109.47 (16)	N(28)−Mo(1)-O(1)		81.0 (3)
N(28)−Mo(1)-S(21)	78.31 (4)			S(28)−Mo(1)-S(21)	80.21 (3)	
O(28)−Mo(1)-O(21)		77.69 (4)	78.59 (9)	N(28)−Mo(1)-N(21)		75.62 (10)

Scheme 2. Reactions of **4** with Bidentate Aromatic Ligands

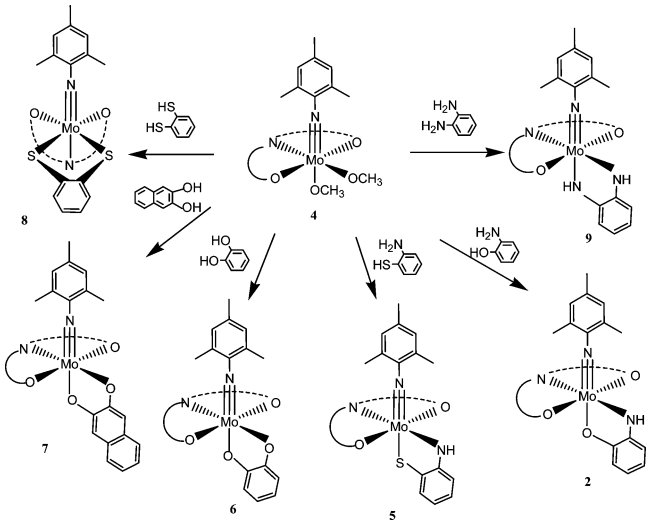

a 1:1 ratio because purer products were obtained using this ratio. Another way to form the imido−amido complexes is by imine metathesis between $Mo(NAr)_2$(sap) and $sapH_2$.[24] The resulting Mo(NAr)(=NC_6H_4OH)(sap) complexes could then rearrange into **1**−**3**.

Compound **4** also reacts with 2-aminothiophenol to form Mo(NAr)(1,2-SC_6H_4NH)(sap), **5**; with catechol to form Mo(NAr)(1,2-OC_6H_4O)(sap), **6**; with naphthalene-2,3-diol to form Mo(NAr)(naphthalene-2,3-diolate)(sap), **7**; with benzene-1,2-dithiol to form Mo(NAr)(1,2-SC_6H_4S)(sap), **8**; and with 1,2-phenylenediamine to form Mo(NAr)(1,2-HNC_6H_4NH)(sap), **9** (Scheme 2). The structures of complexes **5**−**9** have been determined. The crystallographic data are listed in Table 1, and selected bond lengths and bond angles are in Table 3. All complexes show some disorder regarding the sap ligand. Molecular drawings of compounds **6** and **8** are shown in Figures 3 and 4. With the exception of **8**, the structures of the complexes are similar to those of **1**, **2**, and **3**. The coordinating atoms of the bidentate ligand occupy one equatorial and one axial position. In **5**, the amido nitrogen of 2-aminothiophenol is bound in the equatorial position, as in **1**, **2**, and **3**. We synthesized **7** to be able to compare its structure with the corresponding oxo complex, MoO(naphthalene-2,3-diolato)(sap).[15] The coordination spheres differ. In the oxo complex, sap binds in *fac* rather than in *mer* positions,[15] resulting in dihedral angles of 23.5° and 29.5°

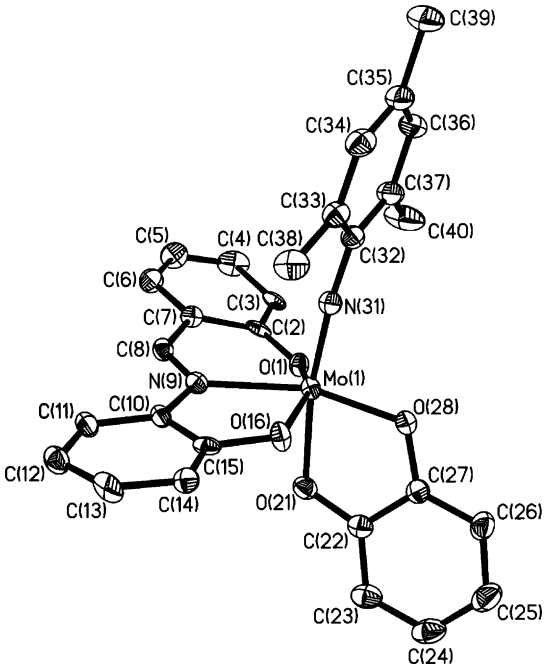

Figure 3. Molecular drawing of Mo(N(2,4,6-Me_3)C_6H_2)(1,2-OC_6H_4O)(sap), **6**.

(24) Cantrell, G. K.; Meyer, T. Y. *Organometallics* **1997**, *16*, 5381. Cantrell, G. K.; Meyer, T. Y. *J. Chem. Soc. Chem. Commun.* **1997**, 8035. Cantrell, G. K.; Meyer, T. Y. *J. Am. Chem. Soc.* **1998**, *120*, 8035.

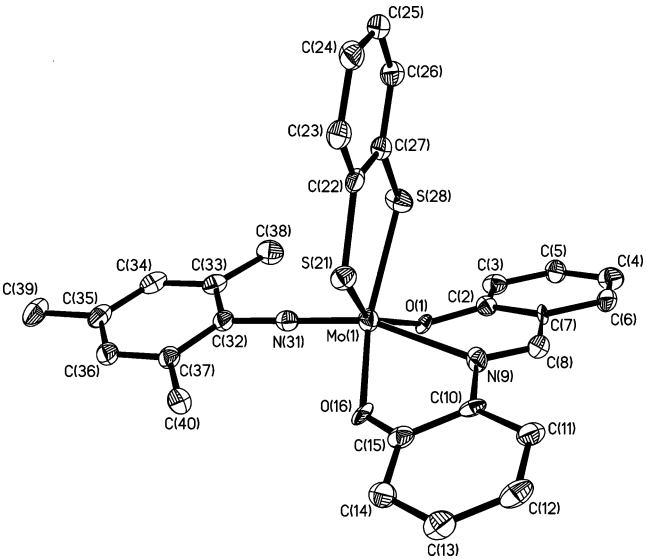

Figure 4. Molecular drawing of Mo(N(2,4,6-Me_3)C_6H_2)(1,2-SC_6H_4S)-(sap), **8**.

Table 4. Selected Bond Lengths (Å) and Bond Angles (°) for **10**

Mo(1)−O(17)	1.6988 (15)	O(17)−Mo(1)−O(16)	97.35 (8)
Mo(1)−O(18)	1.7123 (16)	O(18)−Mo(1)− O(16)	95.66 (8)
Mo(1)−O(1)	1.9242 (17)	O(17)−Mo(1)−N(9)	90.27 (7)
Mo(1)−O(16)	1.9948 (17)	O(17)−Mo(1)−N(9′)	91.2 (6)
Mo(1)−N(9)	2.2800 (19)	O(18)−Mo(1)−N(9)	162.55 (8)
Mo(1)−N(9′)	2.27 (3)	O(18)−Mo(1)−N(9′)	159.9 (7)
Mo(1)−O(19)	2.322 (18)	O(1)−Mo(1)−N(9)	81.95 (7)
O(17)−Mo−O(18)	105.24 (8)	O(1)−Mo(1)−N(9′)	62.3 (8)
O(17)−Mo−O(1)	99.99 (8)	O(17)−Mo(1)−O(19)	173.19 (7)
O(18)−Mo(1)−O(1)	102.69 (8)	O(18)−Mo(1)−O(19)	81.39 (7)

of the phenolates in the sap ligand. In the imido complexes, the phenolates are coplanar. The bond lengths of the imine carbon to the imine nitrogen and to the phenyl carbon of sap in both complexes are comparable. The structure of **8** is similar to that of MoO(naphthalene-2,3-diolato)(sap). It is the only imido complex synthesized here in which the bidentate aromatic ligand has both binding sites in equatorial positions and the nitrogen from sap is located trans to the imido nitrogen. The Mo−imido nitrogen distance in **8** is the shortest of all complexes studied here (1.734(2) Å).

If a solution containing **4** is exposed to moisture-containing air, orange crystals of MoO_2(sap)(CH_3OH), **10**, form (eq 4). The crystallographic data for **10** are listed in Table 1; selected bond lengths and bond angles, in Table 4. The coordination sphere of the molybdenum is a distorted octahedron with the two terminal oxo groups and the coordinated methanol in *mer* positions, similar to the structures of the dioxo complexes with sap derivatives published earlier.[17,18] The Mo═O stretches for **10** are at 933 and 911 cm^{-1} in the infrared spectrum.

$$\mathrm{Mo(NAr)(sap)(OCH_3)_2}\ (\mathbf{4}) + \mathrm{CH_3OH} + 2\mathrm{H_2O} \rightarrow \mathrm{MoO_2(sap)(CH_3OH)}\ (\mathbf{10}) + 2\mathrm{CH_3OH} + \mathrm{H_2NAr} \quad (4)$$

NMR Data. The ^{1}H NMR data for all complexes are listed in the Experimental Section. The spectra of the complexes **1**, **2**, **3**, and **5** in $(CD_3)_2SO$ show a singlet for the proton bound to the amido nitrogen of the bidentate ligand above 14 ppm. Compound **9** has two broad singlets at 13.15 and 9.69 ppm that can be attributed to the two amido protons. The imine proton from $sapH_2$ becomes more deshielded when the ligand is bound (Table 5). The imine protons of the complexes are found above 9 ppm, and their chemical shifts depend on the bidentate ligand. The shielding increases in the order S,S (benzene-1,2-dithiol) < O,O (naphthalene-2,3-diol) < O,O (catechol) < O,NH(2-aminophenol) < S,NH(2-aminothiophenol) < NH,NH (1,2-phenylenediamine). Compound **4**, containing two methoxides instead of a bidentate ligand, has the most shielded imine proton. The imine protons allow an easy identification of mixtures of these compounds.

Table 5. ^{1}H NMR Chemical Shifts of the Sap Imine Proton

compd	δ (ppm) in $(CD_3)_2SO$
1 (NH, O)	9.56
2 (NH, O)	9.51
3 (NH, O)	9.56
4 $(OCH_3)_2$	9.16
5 (NH, S)	9.47
6 (O, O)	9.69
7 (O, O n)	9.73
8 (S, S)	9.92
9 (NH, NH)	9.46
10 (dioxo)	9.26
$sapH_2$	8.70

The consistent presence of six methyl protons in the methanol region of the ^{1}H NMR spectrum allowed the formulation of **4** as a dimethoxide complex. On the basis of COSY spectra, the aromatic protons for **2** and **4** are assigned in Figure 5. The aromatic protons of the 2-amidophenolate in **2** and the imido protons in both complexes are more shielded than the sap protons.

In the compounds with the 2,4,6-trimethylimido ligand, the protons from the methyl group in the p position are more

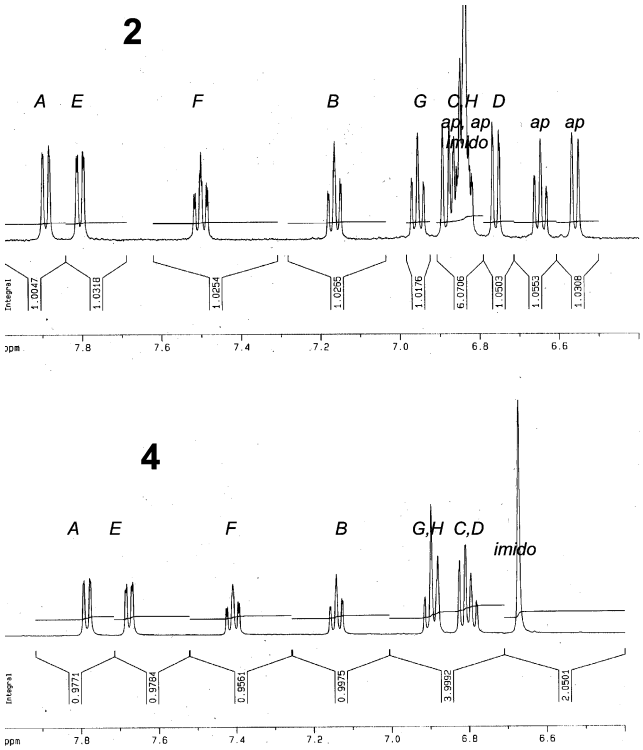

Figure 5. Aromatic regions of the proton NMR spectra of **2** and **4**; the sap protons are labeled according to Figure 1; imido = aromatic protons from the imido ligand, ap = protons from the 2-amidophenolate.

Table 6. Redox Potentials of Compounds **1**−**10** in CH_3CN, 0.2 M TBAHFP

compd	$E^{\circ\prime}$ (V vs Fc^+/Fc)	E_ps(V vs Fc^+/Fc)
1 (NH, O)	−1.37	−2.03
2 (NH, O)	−1.40	−2.06
3 (NH, O)	−1.37	−2.03
4 $(OCH_3)_2$[a]	−1.10	−2.17
5 (NH, S)	−1.20	−1.93
6 (O, O)	−0.85	−1.90 ($E^{\circ\prime}$)
7 (O, O n)	−0.73	−1.86 ($E^{\circ\prime}$)
8 (S, S)	−0.85	−1.87
9 (NH, NH)	−1.55	−2.06
10 (dioxo)[a]	−1.16 (E_p)	−1.99

[a] Two smaller, irreversible peaks follow the first reduction.

Table 7. UV-Vis Absorption Spectral Data of Compounds **1**−**10** in CH_3CN

compd	λ_{max} (nm)	ϵ (M^{-1} cm^{-1})
1 (NH, O)	520	15 000
2 (NH, O)	520	15 000
	350 (sh)	21 000
3 (NH, O)	510	15 000
4 $(OCH_3)_2$	390 (sh)	24 000
	350 (sh)	27 000
5 (NH, S)	550 (sh)	13 000
	420 (sh)	32 000
	350	∼50 000
6 (O, O)	610	9 000
	360	20 000
7 (O, O n)	420 (sh)	27 000
	360	40 000
8 (S, S)	600 (sh)	3 000
	410 (sh)	12 000
	355	23 000
9 (NH, NH)	475 (sh)	26 000
	380 (sh)	42 000
10 (dioxo)	420	8 500

deshielded than the protons from the methyl groups in the o position, except in complex **8**, in which the protons in the o positions are more deshielded.

The three methanol protons in **10** appear in two singlets of approximately equal intensity at 3.14 and 3.16 ppm. This is probably due to the replacement of CH_3OH with $(CD_3)_2SO$ (eq 5).[16]

$$MoO_2(sap)(CH_3OH) + (CD_3)_2SO \leftrightarrow MoO_2(sap)(CD_3)_2SO + CH_3OH \quad (5)$$

Electrochemical and UV−Vis Absorption Data. The electrochemical data for all compounds are listed in Table 6, and the UV−vis absorption data, in Table 7. The imido complexes have one reversible and one generally irreversible reduction between 0 and −2.1 V (Figures 6 and 9). The reversibility of the second peak depends on the bidentate ligand, the scan rate, and the temperature. The second reduction is reversible for compounds **6** and **7** at −25 °C or at scan rates higher than 200 mV/s at room temperature. Complex **7** has the most positive reduction potential of the complexes studied here; complex **9** has the most negative. Since nitrogen is a good σ donor, it is not surprising that **9** is least likely to accept an electron, whereas **7**, with two electronegative oxygen atoms attached to a naphthalene ring, can be reduced more easily. Complex **8** with two sulfurs on the bidentate ligand has the same potential as complex **6** with two oxygen atoms. This is unexpected, but can be attributed to the structural differences between the two compounds. The benzene-1,2-dithiolate in **8** occupies two equatorial positions, whereas the bidentate ligands in all other cases bind in an equatorial and an axial position. It is also interesting to note that the complexes with the most positive first reduction potentials have imido linkages with angles close to 180°, and the complexes with more negative potentials have angles around 166°.

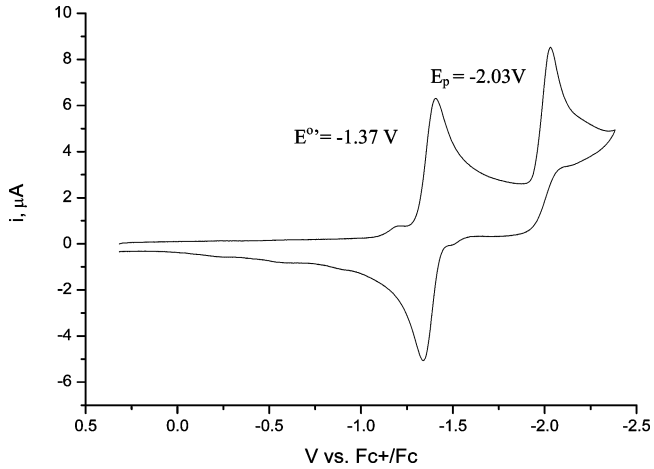

Figure 6. Cyclic voltammogram of **1** in CH_3CN, 0.2 M TBAHFP; sweep rate, 100 mV.

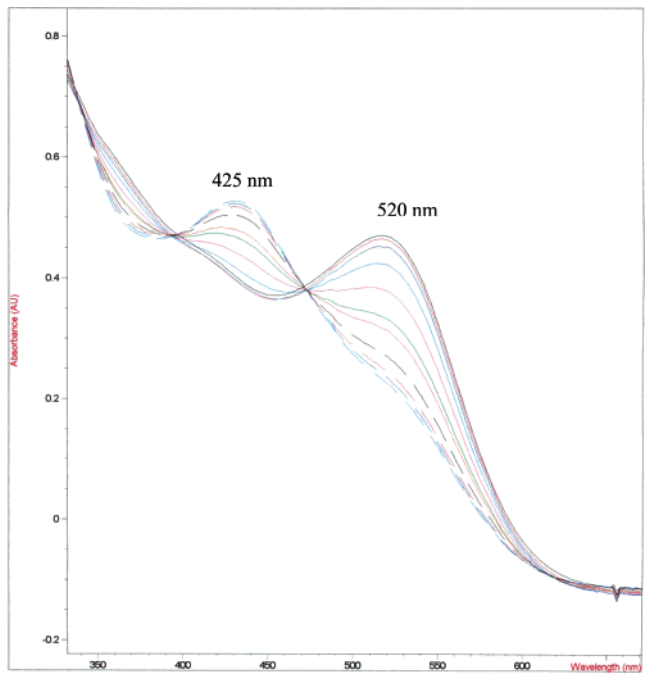

Figure 7. UV−vis absorption data from the spectroelectrochemistry of **1** in CH_3CN, 0.1 M TBATFB.

Using spectroelectrochemistry, we were able to establish that the reversible reduction is a direct one-electron reduction from Mo(VI) to Mo(V). Figure 6 shows the cyclic voltammogram of compound **1**. The changing visible spectra during the gradual reduction of complex **1** can be seen in Figure 7. Plots of $E_{applied}$ vs log[O]/[R] show that the reduction is a one-electron reduction.[20] Solutions of the complexes can also be reduced with sodium amalgam to yield Mo(V) species

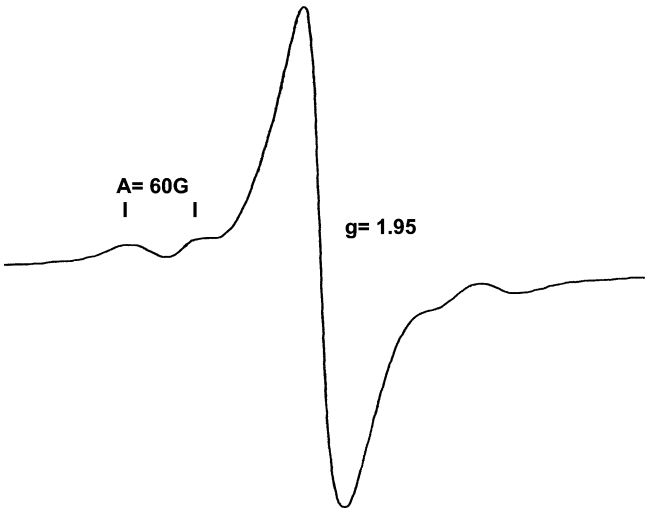

Figure 8. Room temperature EPR spectrum of the Mo(V) derivative of **1**.

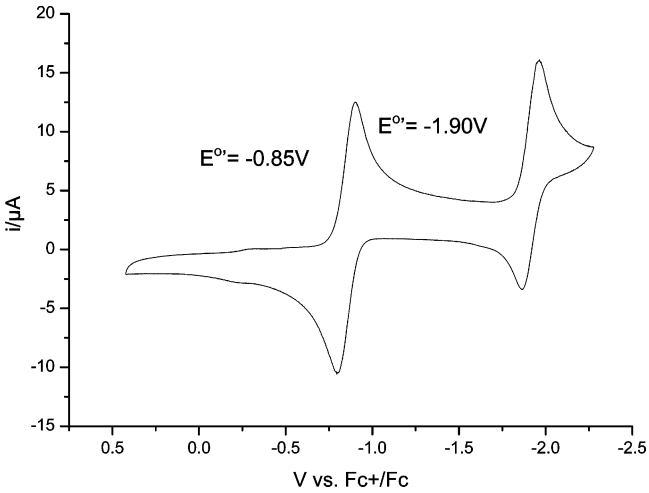

Figure 9. Cyclic voltammogram of **6** in CH_3CN, 0.1 M TBAHFP; sweep rate, 400 mV/s; −25 °C.

with the same visible spectra as those obtained from the spectroelectrochemistry experiment. A room temperature EPR spectrum of the chemically reduced **1** is shown in Figure 8. The g value of 1.95 is typical for Mo(V) complexes with nitrogen- and oxygen-containing ligands.[25,26]

A cyclic voltammogram of **6** is shown in Figure 9. The second reduction of **6** is completely reversible at −25 °C and was determined to be a one-electron reduction. Visible spectra of **6** before the reduction, after the one-electron reduction, and after the two-electron reduction are shown in Figure 10. After the first reduction, the solution shows an EPR signal with a g value of 1.960 (Figure 11). The EPR signal decreases to <5% of its original size after the second reduction. The reduced complex can be reoxidized to the starting material. On the basis of the ϵ values, the electronic transitions are ligand-to-metal charge-transfer bands.

The oxo complex MoO(naphthalene-2,3-diolate)(sap), like the imido compounds studied here, shows a reversible one-

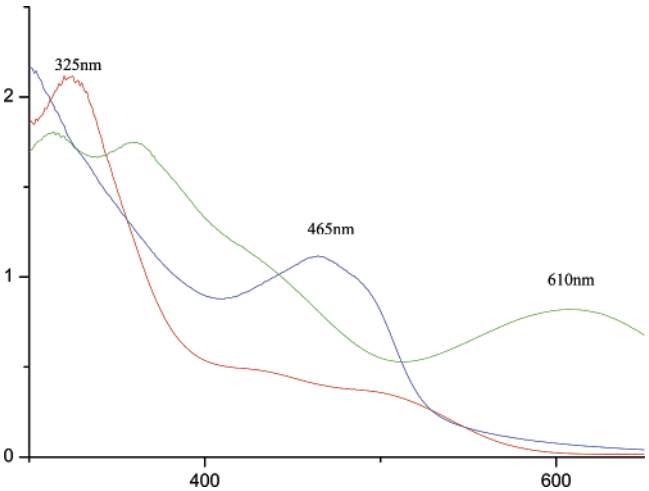

Figure 10. UV−vis absorption spectra of **6** before (green) and after the reduction with one electron (blue) and after the reduction with two electrons (red).

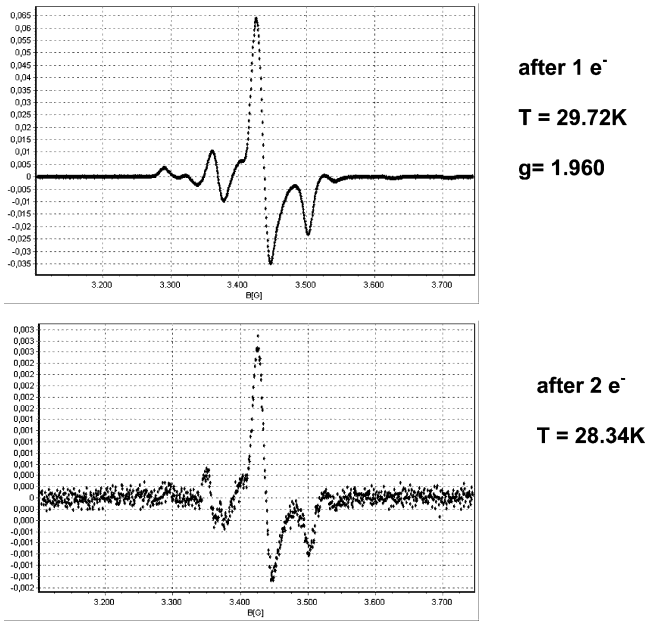

Figure 11. EPR spectra of **6** after a one-electron reduction and after a two-electron reduction.

electron reduction, but the potential is significantly more positive,[15] as one would expect with a more electronegative, multibonded ligand. A second reduction peak is also present in the cyclic voltammogram of the oxo complex. It becomes more reversible with increasing sweep rate. This second reduction peak is found not only in the Mo(VI) monooxo and -imido complexes but also in Mo(VI) dioxo complexes, MoO_2(sap)(S) (S = Lewis base solvent),[16] and Mo(IV) oxo complexes, MoO(sap)(S).[27] It could represent a reduction from Mo(V) to Mo(IV)[15] or a reduction of the sap ligand. The fact that this peak is also found in the cyclic voltammogram of Mo(IV) oxo complexes supports the latter interpretation. The cyclic voltammogram of the Mo(IV)) complex has an irreversible oxidation peak. Even if the scan is started at a more negative potential than the oxidation potential from Mo(IV) to Mo(V),[27] the reduction peak is still

(25) Scullane, M. I.; Taylor, R. D.; Minelli, M.; Spence, J. T.; Yamanouchi, K.; Enemark, J. H.; Chasteen, N. D. *Inorg. Chem.* **1979**, *18*, 3213.
(26) Xiao, Z.; Bruck, M. A.; Doyle, C.; Enemark, J. H.; Grittini, C.; Gable, R. V.; Wedd, A. G.; Young, G. C. *Inorg. Chem.* **1995**, *34*, 5950.
(27) Boyd, I. W.; Spence, J. T. *Inorg. Chem.* **1982**, *21*, 1602.

present. This interpretation is consistent with the EPR results for **6**, since the lone electron from the reduction of sip can couple with the electron from the Mo(V), leading to a disappearance of the EPR signal.

Compound **10** has two smaller irreversible peaks following the first reduction peak at −1.16 V and a peak at −1.99 V. The potentials are comparable to data from the literature.[16]

Conclusions

The reaction of $Mo(NAr)_2Cl_2(dme)$ with $sapH_2$ leads to the formation of imido−amido complexes, $Mo(NAr)(1,2\text{-}OC_6H_4NH)(sap)$. The compounds are formed via an intermediate, $Mo(NAr)(sap)(OCH_3)_2$, which has been isolated. This intermediate can be reacted with bidentate aromatic ligands to form complexes in which, with the exception of the 1,2-benzenedithiolate complex, the bidentate ligand occupies an equatorial and an axial position. The Mo(VI) in the compounds can be reversibly reduced to an EPR-active Mo(V). The reduction potentials depend on the bidentate ligand. A second, generally irreversible one-electron reduction is reversible for the catecholate and naphthalene-2,3-diolate complexes. Complexes with more positive first reduction potentials tend to have imido linkages with angles close to 180°.

Acknowledgment. We thank Grinnell College for financial support of this research. M.M. thanks the University of Konstanz and especially Prof. P. Kroneck for the opportunity to spend July 2004 as a visiting professor there and work on this project. M.M. gives special thanks to Professor K. Wieghardt at the Max-Planck Institute for Bioinorganic Chemistry, Mülheim (Ruhr), for the opportunity to spend a sabbatical semester there in the fall of 2005.

Supporting Information Available: CIF file of crystallographic data. This material is available free of charge via the Internet at http://pubs.acs.org.

IC060370+